Macromolecules

Article

pubs.acs.org/Macromolecules

Metastable Knots in Confined Semiflexible Chains

Liang Dai,[†] C. Benjamin Renner,[‡] and Patrick S. Doyle*[,†,‡]

[†]BioSystems and Micromechanics (BioSyM) IRG, Singapore-MIT Alliance for Research and Technology (SMART) Centre, Singapore 138602

[‡]Department of Chemical Engineering, Massachusetts Institute of Technology, Cambridge, Massachusetts 02139, United States

Supporting Information

ABSTRACT: We study the size distribution of spontaneous knots on semiflexible chains confined in square cross-section channels using Monte Carlo simulations. The most probable knot size, i.e. the metastable knot size, is found to vary nonmonotonically with the channel size. In the case of weak confinement, the metastable knot size is larger than the knot size in bulk because the segments within the knot feel less channel confinement than the segments outside the knot, and the channel pushes the segments into knot cores to reduce the overall free energy. Conversely, in the case of strong confinement, the metastable knot size is smaller than the one in bulk because the segments within the knot experience more channel confinement, and the channel expels segments from the knot core. We demonstrate that a simple theory can capture this nonmonotonic behavior and quantitatively explain the metastable knot size as a function of the channel size. These results may have implications for tuning the channel size to either generate or screen knots.

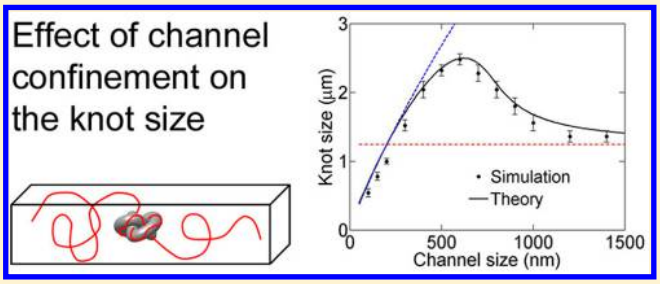

1. INTRODUCTION

Long linear polymers both tie and untie "knots" through the random motions of the chain.[1] These types of knots have been shown to affect the mechanical,[2,3] rheological,[4,5] and structural properties of polymer molecules. In biological contexts, knots have been found in proteins[6] and viral capsid DNA.[7] Experiments and simulations have begun to address the structure of a knot along a polymer in a good solvent—some experiments[8] and simulations[9] have suggested the localization of a knot whereas other simulations have suggested the opposite.[10,11] For semiflexible polymers like DNA, Grosberg and Rabin posited that a competition between bending and confinement energies within a knotted region of the chain results in a localized, metastable knot for long, thin polymers.[12] The metastable knot corresponds to a local minimum in the free energy landscape with respect to the knot size. In a recent publication, we validated the existence of metastable knots in semiflexible chains with computer simulations and extended the Grosberg–Rabin (GR) theory to incorporate the effect of a finite chain width.[13] We also investigated the existence of metastable knots in flexible chains, i.e., in the absence of bending energy.[14]

Advances in microfabrication have spurred fundamental experimental research into the static and dynamic properties of double-stranded DNA (dsDNA) in microfluidic confinement.[15,16] Computer simulations have systematically investigated the scaling regimes of a confined polymer,[17−21] and experiments have added support to these arguments for both static and dynamic properties.[22−27] More recently, the topological properties of polymers in confinement have been investigated. Simulation results have indicated that the probability of forming a knot can depend nonmonotonically on the degree of confinement in slits[28,29] or channels.[30,31] The most direct experimental measurements of knot sizes have been on actin[32] and DNA[33] held under tension by optical tweezers. Knotted DNA molecules have been observed in nanochannels,[34] and confinement could provide a passive means of visualizing the size of knots in polymers. Beyond these fundamental studies, nanochannels have been used to extend dsDNA for the optical mapping of genomes,[35−37] and knots may have been observed to interfere with this process by reducing apparent separation between sites.[38]

In the current study, we analyze how confining a knotted polymer in a channel may affect the size of the knot. Previous studies have observed a nonmonotonic trend in knot size upon increasing confinement.[29,30] Here, we investigate the physical mechanism behind these observations with both simulations and theory. We modify the GR theory to incorporate the effect of confinement in a channel, leading to a theory for the size distribution of knots along chains confined in channels. This modified theory predicts a nonmonotonic variation of the knot size with the confining dimension. We tested this theory with detailed Monte Carlo simulations to sample trefoil knot configurations along chains confined within channels. Our results demonstrate the modified GR theory quantitatively agrees with the metastable knot size from simulations, and we provide predictions for the sizes of channels where the theory can be tested with dsDNA experiments.

Received: February 9, 2015
Revised: April 2, 2015
Published: April 14, 2015

DOI: 10.1021/acs.macromol.5b00280
Macromolecules 2015, 48, 2812−2818

2. THEORY AND SIMULATION

2.1. Theory for the Metastable Knots. Let us first recall the modified GR theory for semiflexible polymers with finite thickness in bulk (no confinement). The free energy cost of knot formation in bulk follows

$$F_{knot}^{bulk}(L_{knot}) = k_1\left(\frac{L_{knot}}{L_p}\right)^{-1} + k_2 L_{knot}(L_{knot} - pw)^{-2/3} L_p^{-1/3} \quad (1)$$

where L_{knot} is the contour length in the knot, L_p is the persistence length, and w is the chain width. The numerical coefficients $k_1 = 17.06$, $k_2 = 1.86$, and $p = 16$ were determined for trefoil knots in the previous study.[13] The first term represents the bending energy due to the increased curvature of the contour within the knot, and the second term corresponds to the confinement free energy within the knot resulting from topological constraints. Note that eq 1 only contains terms involving L_{knot} because our primary purpose is to calculate the size distribution of knots from the free energy.

For semiflexible chains in square channels, the free energy cost of knot formation using the diagram of states, illustrated in Figure 1a, is approximated as

$$F_{knot}^{channel}(L_{knot}) = F_{knot}^{bulk}(L_{knot}) + F_{knot}^{wall}(L_{knot}) - F_{unknot}^{wall}(L_{knot}) \quad (2)$$

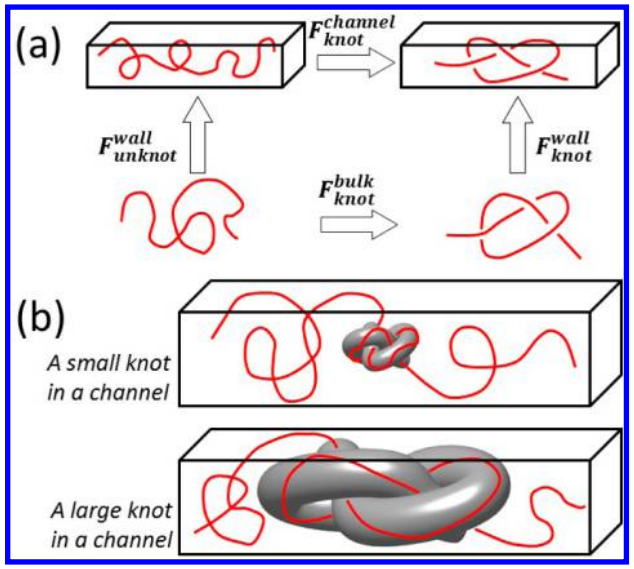

Figure 1. (a) A diagram to show the free energy difference between four states: an unknotted subchain in bulk, a knotted subchain in bulk, an unknotted subchain in a channel, and a knotted subchain in a channel. (b) Illustrations of small (top) and large (bottom) knots confined in a channel.

where $F_{knot}^{wall}(L_{knot})$ corresponds to the free energy cost of confining a knot while the contour length of the knot is maintained as L_{knot} and $F_{unknot}^{wall}(L_{knot})$ corresponds to the confinement free energy of an unknotted chain with contour length L_{knot}. Note that in the definition of $F_{knot}^{wall}(L_{knot})$ we ignore the confinement free energy experienced by the unknotted portion $(L - L_{knot})$ in a knotted chain because this contribution would cancel with an identical term in F_{unknot}^{wall}. It is also worth pointing out that writing the free energy as in eq 2, we make the approximation that the free energies of knotted and unknotted portions do not affect each other. In the real case, the knotted and unknotted subchains may penetrate each other, which could modify the free energy. For simplicity, such effects are not included. For convenience, we define an excess free energy

$$F_{excess}(L_{knot}) \equiv F_{knot}^{wall}(L_{knot}) - F_{unknot}^{wall}(L_{knot}) \quad (3)$$

Equation 2 then becomes

$$F_{knot}^{channel} = F_{knot}^{bulk} + F_{excess} \quad (4)$$

Rewriting eq 2 in this way enables a simple physical interpretation of how the confining geometry interacts with the knotted subchain. When the knotted region of the chain experiences more confinement free energy due to the channel walls than the unknotted region of the chain, i.e. $F_{excess} > 0$, forming a knot is more difficult inside the channels than in bulk, and the formation of the knot becomes less likely. Conversely, in situations where the unknotted region of the chain experiences more confinement free energy due to the walls than the knotted region of the chain, i.e. $F_{excess} > 0$, forming a knot becomes more likely within the confining geometry.

Now, we turn to calculate F_{excess}. The term $F_{unknot}^{wall}(L_{knot})$ can be approximated as the confinement free energy of equilibrium chains in channels $F_{chain}(L_{knot})$, which is ensemble-average of knotted and unknotted chains. This approximation is based on the fact that knots usually occur in small portions of a long chain. The functional form of $F_{chain}(L_{knot})$ depends on the strength of confinement. For certain regimes, scaling expressions exist for this term. For example, in the tightly confined Odijk regime ($D \ll L_p$), the chain periodically deflects off the confining walls, leading to an expression with the same form as the second term in eq 1. In the de Gennes regime ($L_p \ll D \ll R_{bulk}$), where R_{bulk} is the radius of gyration of the chain in bulk, the chain partitions itself into a series of self-avoiding blobs of size D. In the current study, we mainly deal with confining channels in the de Gennes regime $L_p \ll D \ll R_{bulk}$, leading to

$$F_{unknot}^{wall}(L_{knot}) = 5.0 D^{-5/3} w^{1/3} L_p^{1/3} L_{knot} \quad (5)$$

where the prefactor 5.0 was determined in a previous study.[17] As the strength of confinement crosses over to the Odijk regime ($D \ll L_p$), eq 5 starts to underestimate the confinement free energy.[17]

The term $F_{knot}^{wall}(L_{knot})$ depends on the size of the knot relative to that of the channel. When the knot size is much smaller than the channel size, referred to as the "small" knot regime, the knot is weakly deformed and can be considered as a ball with an effective diameter b_{knot}. The term b_{knot} is approximately proportional to L_{knot}, so we write $b_{knot} = \alpha L_{knot}$, where α is a numerical coefficient less than 1. The confinement free energy of this ball is approximated as the one for a bead on a flexible chain of identical balls.[39] Then, we have $F_{knot}^{wall}(L_{knot}) \approx b_{knot}^{5/3}(D - b_{knot})^{-5/3}$. In the expression, $(D - b_{knot})^{-5/3}$ is used in favor of $D^{-5/3}$ because the center of the knot-ball is restricted in a channel of size $(D - b_{knot})$ due to the finite thickness of the ball. After introducing a numerical coefficient β, we obtain

$$F_{knot}^{wall}(L_{knot}) = \beta L_{knot}^{5/3}(D - \alpha L_{knot})^{-5/3} \quad (6)$$

When the knot size is much larger than the channel size, referred to as the "large" knot regime, we can consider the different portions of the knot to be confined in many

DOI: 10.1021/acs.macromol.5b00280
Macromolecules 2015, 48, 2812−2818

subchannels with channel size less than D, discussed by Nakajima and Sakaue[31] and shown in Figure 1b. In such a situation, the contour within the knot experiences a larger confinement free energy penalty than outside the knot.

In the current study, we will use eq 4 with eq 5 and eq 6 to calculate the metastable knot size in channels because the metastable knot size is usually located in the "small" knot regime for the channel sizes in this study.

2.2. Polymer Model and Simulation Method. We performed Monte Carlo simulations of polymers confined in square cross-section channels to test the preceding theoretical predictions. Polymer chains were modeled as a string of touching beads. The diameter of each bead corresponds to the effective chain width w, and the contour length L follows as $L = (N-1)w$, where N is the number of beads. The present model contains only three interaction energies: pairwise hardcore repulsion between beads, hardcore repulsions between the beads and the channel walls, and a harmonic bending energy $E_{bend}(\theta)/k_BT = (1/2)(L_p/w)\theta^2$ used to reproduce the persistence length L_p.

Configurations of chains were sampled with a standard Monte Carlo procedure.[18] Each Monte Carlo cycle consisted of alternating crankshaft or reptation moves. For a given set of parameters, we typically performed 10^{11} cycles and sampled the chain configuration every 1000 cycles. For each parameter set, the number of knotted chains was approximately 10^6 or 10^7, resulting in knotting probabilities between 0.01 and 0.1 for our simulation conditions.

Since the topology of an open chain is not well-defined, the chains must be systematically "closed" in order to determine its topology. In the current study, the closing loop is generated by minimally interfering closure scheme.[40] After closing the chain, the topology of the chain is determined by calculating the Alexander polynomial.[41] Further details about the determination of knot size are presented in our previous publication.[13] Note that the knots of open chains might be ambiguous when the knot size is close to the entire chain. However, knots can be easily distinguished from unknots, when the knot size is much less than the entire chain. In the current study, the contour lengths of metastable knots are usually 1 order of magnitude less than the entire chain, and hence these knots are well-defined.

3. RESULTS AND DISCUSSION

The probability distributions of trefoil knot sizes for semiflexible chains confined in channels of varying sizes as well as in bulk are shown in Figure 2. The contour length is fixed as $L = 400L_p$, and the chain width is fixed as $w = 0.4L_p$. For each curve, the probability $f(x)$ is normalized such that $\int_0^{L/L_p} f(x)\,dx = f_{total}$, where $x = L_{knot}/L_p$ and f_{total} is the total probability of forming a trefoil knot on the chain. For all channel sizes as well as the bulk case, the probability distribution attains a maximum at L^*_{knot}, indicating a metastable knot. The shapes and magnitudes of the probability distributions of knot size are markedly influenced by confinement, and the metastable knot size L^*_{knot} depends on the channel size. We note that we focus the present analysis on the metastable knot size L^*_{knot} rather than the average knot size $\langle L_{knot}\rangle$, the latter which has been the primary quantity analyzed in other studies of knot size.[29−31,42] For the present study, examining L^*_{knot} is preferable for two reasons: (i) free energy arguments are more directly manipulated to give an estimate of L^*_{knot}, and (ii) L^*_{knot} is relatively insensitive to the contour length of the molecule while $\langle L_{knot}\rangle$ is strongly affected by the contour length due to the long tail of the knot size distribution (see Supporting Information).

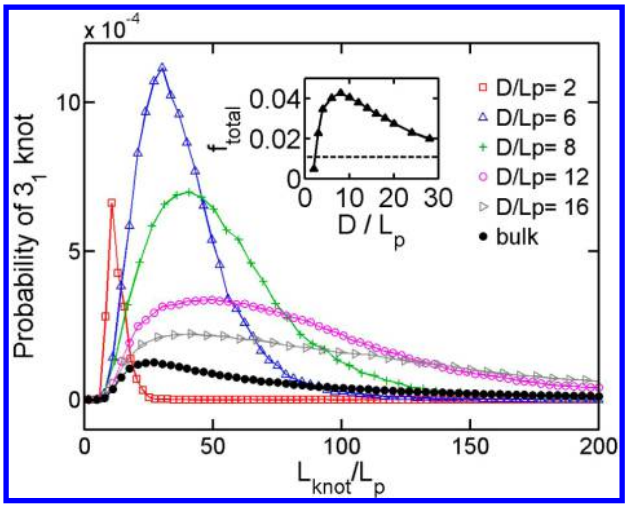

Figure 2. Probability distributions of the sizes of trefoil knots for different confining channel widths, D. For all curves, the contour length is fixed as $L = 400L_p$, and the chain width is fixed as $w = 0.4L_p$. The inset shows the total probability of trefoil knots as a function of channel size. The dashed line in the inset shows the probability of trefoil knots in bulk.

The total probability of forming a trefoil knot as a function of the channel size is shown in the inset of Figure 2. As the degree of confinement is increased, f_{total} increases from the bulk value 0.011 to the peak value 0.043 at $D = 8L_p$. A further reduction of the channel size causes a sharp decrease in f_{total} to zero. A similar nonmonotonic behavior in knotting probability was also observed in our previous study of circular chains in slits.[28]

The metastable knot size L^*_{knot} also varies nonmonotonically with D, shown in Figure 3. A similar trend has been observed in the previous simulation of confined semiflexible chains.[30] As D decreases, L^*_{knot} increases from the bulk value of $27.2L_p$ to the peak value of $49.6L_p$ at $D = 12L_p$, decreasing rapidly thereafter. The metastable knot sizes shown here are much less than the contour length of the chain $L = 400L_p$; accordingly, the end effects due to finite chain length are weak. To rule out the possibility that the nonmonotonic change of L^*_{knot} versus D is caused by entering the weak confinement regime, we identified the de Gennes regime as $4 \le D/L_p \le 20$ by analyzing the

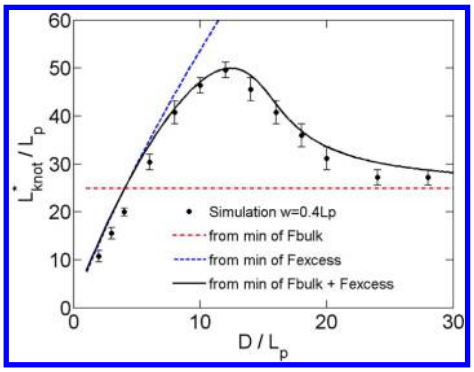

Figure 3. Most probable size of a trefoil knot as a function of the channel size. The solid line corresponds to the minimization of free energy in eq 4 with respect to L_{knot} using numerical coefficients $\alpha = 0.1$ and $\beta = 0.02$. The contour length is fixed as $L = 400L_p$, and the chain width is fixed as $w = 0.4L_p$.

DOI: 10.1021/acs.macromol.5b00280
Macromolecules 2015, 48, 2812−2818

confinement free energy of the chain (see Supporting Information). The peak of L^*_{knot} at $D/L_p \approx 12$ is located well inside the de Gennes regime, so a transition in the effective confinement regimes is not responsible for the nonmonotonic change of L^*_{knot} versus D.

The standard deviation of knot size, σ_{knot}, as a function of the channel size is shown in Figure 4. Fluctuations in the size of the knots monotonically decrease as the channel size is decreased. This result directly reflects the tightening of the distributions of knot sizes shown in Figure 2. In other words, confinement acts to stabilize and more sharply localize the knot on a chain. The data in Figure 4 agree qualitatively with experimental observation of small fluctuations in knot size during the diffusion and escape of a knot along a DNA molecule confined in a channel.[34]

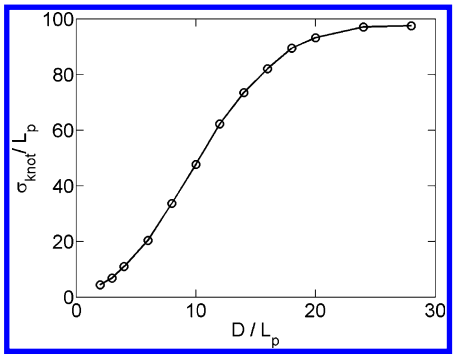

Figure 4. Standard deviation of knot size as a function of the channel size. The contour length is fixed as $L = 400L_p$, and the chain width is fixed as $w = 0.4L_p$.

The average deformation ratio of trefoil knots as a function of the channel size is shown in Figure 5a. The deformation ratio is calculated as $2\langle R_x\rangle/(\langle R_y\rangle + \langle R_z\rangle)$, where $\langle R_x\rangle$, $\langle R_y\rangle$, and $\langle R_z\rangle$ are the radii of gyration in each direction. The x-axis corresponds to the axis of the channel. In the absence of confinement, knots are isotropic, and the average deformation ratio is one. Even in weak confinement, noticeable anisotropy is present in the knotted regions. This result may occur due to deformation of knots located near the channel walls. The deformation ratio increases monotonically as the channel size decreases. When $D \leq 6L_p$, the average deformation ratio increases more sharply. The extensions of knots along the direction of the channel axis are shown in Figure 5b. The extension is defined as the maximum span of the knot projected in the direction of the channel axis. We plot the most probable value of extension $L^*_{\|}$ rather than the mean value of extension $\langle L_{\|}\rangle$ because $L^*_{\|}$ is insensitive the contour length of the chain. The most probable value of extension of the knot is smaller than the channel size for $D > 4L_p$.

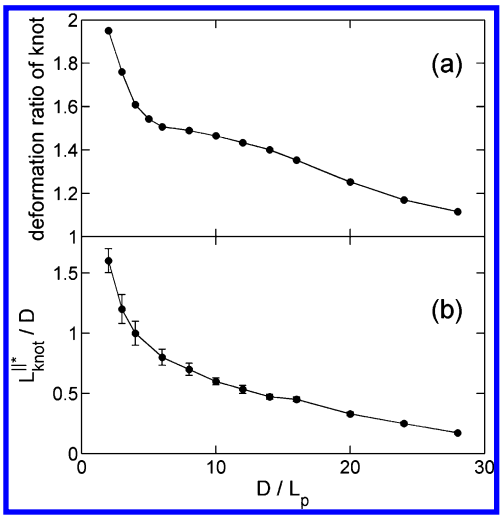

Figure 5. (a) Deformation ratio of knots as a function of the channel size. The deformation ratio is calculated as $2\langle R_x\rangle/(\langle R_y\rangle + \langle R_z\rangle)$, where $\langle R_x\rangle$, $\langle R_y\rangle$, and $\langle R_z\rangle$ are the radii of gyration in each direction. The x-axis corresponds to the axis of the channel. (b) The most probable extension of trefoil knot as a function of the channel size. The contour length is fixed as $L = 400L_p$, and the chain width is fixed as $w = 0.4L_p$.

Next, we compare the metastable knot size in simulations with the theoretical prediction from eq 1, shown by the black curve in Figure 3a. By choosing numerical coefficients $\alpha = 0.1$ and $\beta = 0.02$, our theory is able to quantitatively reproduce the dependence of L^*_{knot} on D, shown in Figure 3. The fitted value of $\alpha = 0.1$ suggests that the effective diameter of knot-ball, b_{knot}, is roughly $0.1L_{knot}$, which is reasonable. After substituting $b_{knot} = 0.1L_{knot}$ into eq 6 with $\beta = 0.02$, we have $F^{wall}_{knot} = 0.93b_{knot}^{-5/3}(D - b_{knot})^{-5/3}$, where the prefactor 0.93 is close to unity.

In our theory, the metastable knot size is determined by the minimum of $F^{wall}_{knot}(L_{knot})$ and $F_{excess}(L_{knot})$ for a given channel size. To further examine our theory, we compare F^{bulk}_{knot} and F_{excess} calculated from simulations and theory. The free energy of knots in bulk F^{bulk}_{knot} as a function of knot size is shown in Figure 6a. The metastable knot size in bulk, F^{bulk}_{knot}*, predicted by eq 1 is 27.2L_p, slightly larger than 24.9L_p observed in the simulations. Note that the calculation of $F^{bulk}_{knot}(L_{knot})$ by eq 1 is no longer valid for very large knots because eq 1 is derived based on the Odijk scaling for self-confinement free energy of knots in bulk, and the Odijk scaling is only valid in strong confinement, i.e., the tight knots.[12,13]

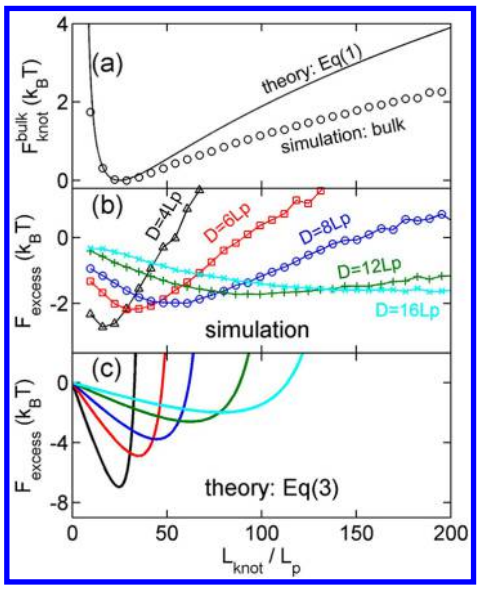

Figure 6. (a) Potential of mean force as a function of knot size for a semiflexible chain in bulk. (b) Difference in confinement free energy, F_{excess}, between a knotted and unknotted subchain as a function of the knot size calculated from simulation. (c) F_{excess} calculated from theory. The contour length is fixed as $L = 400L_p$, and the chain width is fixed as $w = 0.4L_p$.

DOI: 10.1021/acs.macromol.5b00280
Macromolecules 2015, 48, 2812−2818

The values of F_{excess} extracted from simulations of knots are shown in Figure 6b. The value of F_{excess} is extracted using $F_{excess} \equiv F_{knot}^{wall} - F_{nonknot}^{wall} = F_{knot}^{bulk} - F_{knot}^{channel} = \log(f_{channel}) - \log(f_{bulk})$, where $f_{channel}$ and f_{bulk} are the knotting probabilities as a function of L_{knot}, shown in Figure 2. Recall that $F_{knot}^{wall} - F_{nonknot}^{wall} = F_{bulk}^{channel} - F_{knot}^{channel}$ is based on the diagram in Figure 1a. In addition, applying $F_{knot}^{bulk} = -\log(f_{bulk})$ and $F_{knot}^{channel} = -\log(f_{channel})$ is accurate only when the probability of forming a trefoil knot is small and the probabilities of other knots are negligible in comparison. This requirement is satisfied since the probability of forming a trefoil knot is small (<5%), and the probabilities of other knots are always less than 1%.

The theoretical predictions of F_{excess} calculated using eqs 4−6 with the fitted coefficients $\alpha = 0.1$ and $\beta = 0.02$ (determined in the fit of L_{knot}^{*} in Figure 3) are shown in Figure 6c. Our theory qualitatively captures three major features of F_{excess}. First, $F_{excess}(L_{knot})$ exhibits a minimum. Second, the value of L_{knot} at the minimum of F_{excess} decreases with decreasing D. Third, the potential well becomes deeper with decreasing D. Quantitatively, our theoretical predictions of F_{excess} deviate from the ones extracted from simulation, particularly for large L_{knot}. This deviation is caused by two major assumptions in our theory: (i) the knot core is treated as an isotropic ball, and (ii) the effective diameter b_{knot} of the ball is proportional to L_{knot}. The first assumption is not valid for small channels because the knot is significantly deformed as shown in Figure 5a. The second assumption is not valid for large knots, as shown by data of knot radius versus L_{knot} in the Supporting Information.

The insights from Figure 6 enable a deeper understanding of the dependence of L_{knot}^{*} on D in Figure 3. The metastable knot size corresponds to the minimum of $F_{knot}^{channel} = F_{knot}^{bulk} + F_{excess}$. The location of the minimum in F_{knot}^{bulk} is independent of D (red line Figure 3a). The value of L_{knot} which minimizes F_{excess} becomes smaller with the decreasing D (blue line Figure 3a). In wide channels, the confinement effect is weak, $F_{knot}^{channel}$ is dominated by F_{knot}^{bulk}, and thus L_{knot}^{*} is close to the minimum in the bulk value $F_{knot}^{bulk}*$. In narrow channels, $F_{knot}^{channel}$ is dominated by F_{excess}, and L_{knot}^{*} approaches the minimum of F_{excess}. In between these extremes, the competition between F_{knot}^{bulk} and F_{excess} causes the nonmonotonic change in L_{knot}^{*}. Interestingly, although our theoretical predictions of F_{knot}^{bulk} and F_{excess} in Figure 6 are not precise, the prediction of L_{knot}^{*} is significantly more accurate, probably due to cancellation of errors. As shown by Figure 6a, eq 1 overestimates the shrinking force $-\partial F_{knot}^{bulk}/\partial L_{knot}$ of knots when the knot size is larger than the metastable knot size in bulk. On the other hand, as shown by two y-axes in Figures 6b and 6c, eq 3 overestimates the swelling forces $-\partial F_{excess}/\partial L_{knot}$.

The physical reason why the shrinking a knot can reduce the confinement free energy of the knot is that a subchain of L_{knot} is compacted in the knotted region. For the knotted and unknotted states, the confinement free energies scale as $(D - \alpha L_{knot})^{-5/3} L_{knot}^{5/3}$ and $D^{-5/3} w^{1/3} L_p^{1/3} L_{knot}$, respectively. The ratio is $L_{knot}^{2/3}/(w^{1/3} L_p^{1/3})$, if we approximate $(D - \alpha L_{knot}) \approx D$. This ratio approaches zero as the knot size approaches zero. In other words, when the knot is small, the segments inside the knot experience less confinement from the channel walls than the segments outside the knot. As the knot size increases, $L_{knot}^{2/3}/(w^{1/3} L_p^{1/3})$ eventually becomes larger than 1. This means that when the knot is large, the segments inside the knot experience more confinement from the channel walls than the segments outside the core of the knot. Furthermore, as the knot size increases, the term $D/(D - \alpha L_{knot})$ increases to an infinitely large value, which corresponds to a large ball without transitional freedom in the cross-section of the channel. The knotted region, however, is a soft ball rather than a hard ball. Thus, the entropy gained from deformability becomes the dominant effect.

It is worth mentioning that we assume the knot core to be undeformed from equilibrium in order to express the free energy in two terms: $F_{knot}^{bulk}(L_{knot})$ in eq 1 and $F_{knot}^{wall}(L_{knot})$ in eq 6. However, the confining channel will deform the knot core from a spherical shape, and this deformation will affect both $F_{knot}^{bulk}(L_{knot})$ and $F_{knot}^{wall}(L_{knot})$. As mentioned in the previous paragraph, the deformation should provide more translational freedom for the knot core in the transverse directions. This deformation will affect $F_{knot}^{bulk}(L_{knot})$ due to the change in p—a parameter in eq 1 to describe the aspect ratio of the maximally inflated virtual tube of a knot.[13] Figure 5a shows that the deformation ratio is always less than 2 for the tube diameters $D \geq 2L_p$. For simplicity, the effects of deformation on $F_{knot}^{bulk}(L_{knot})$ and $F_{knot}^{wall}(L_{knot})$ are not considered in the theoretical framework of the current study.

The results in Figures 2−6 are for confined semiflexible chains with the chain width $w = 0.4L_p$ and contour length $L = 400L_p$. To investigate the effect of changes in chain width on the agreement between simulation and theory, we performed simulations for confined semiflexible chains with chain widths $w = 0.2L_p$ and $w = 0.1L_p$. The black circle in Figure 7 shows the

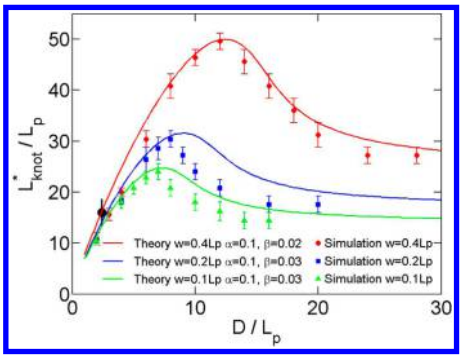

Figure 7. Metastable knot size as a function of channel size for different chain widths. The symbols and lines correspond to simulation results and theoretical predictions, respectively. The contour lengths are fixed as $L = 400L_p$. The black circle shows the previous simulation result[30] of a chain with $L = 4.8$ μm, $L_p = 50$ nm, and $w = 2.5$ nm confined in a channel with size of $D = 240$ nm.

metastable knot size in the previous simulation study[30] of a confined chain with the parameters $L = 96L_p$, $w = 0.05L_p$, and $D = 2.4L_p$. Our results are in reasonable agreement with previous result. The metastable knot sizes for three different chain widths are compared to our theoretical predictions in Figure 7. Recall that our theory requires two numerical coefficients α and β. For $w = 0.4L_p$, we use the coefficients $\alpha = 0.1$ and $\beta = 0.02$ to attain agreement between theory and simulation. For $w = 0.2L_p$ and $w = 0.1L_p$, we maintain $\alpha = 0.1$ and change β to 0.03 in order to match our theory to simulation results. The coefficient α is used to relate the effective diameter of the knot, b_{knot}, and the contour length of the knot, L_{knot}. Our simulation results show that the relationship between b_{knot} versus L_{knot} is insensitive to the chain width (see Supporting Information), and thus the value of α is independent of the chain width. The reason why we change β for different chain widths is as follows. The theoretical equation for F_{knot}^{bulk} (eq 1) is fairly accurate for thin chains (see Supporting Information and ref 13) but

DOI: 10.1021/acs.macromol.5b00280
Macromolecules 2015, 48, 2812−2818

significantly overestimates the force which shrinks a knot for thick chains (Figure 6a). To compensate for this overestimation, we need to similarly overestimate the swelling force due to F_{excess}. Therefore, the value of β used in eq 6 is larger for thinner chains.

Our theory is able to capture three major trends concerning the dependence of L^*_{knot} on w and D, shown in Figure 7. First, as w decreases, the peak value decreases. Second, as w decreases, the peak in L^*_{knot} shifts to smaller channel sizes. Third, for all w, the curves of L_{knot} versus D converge at very small channel sizes.

4. CONCLUSIONS

We have used computer simulations to show how confinement in a channel may alter the sizes and probabilities of formation of knots in polymer molecules. We put these simulation results in context of a theory that explains the physics of the process: the competition between bending energy within the knot and confinement energy within the knot and due to the channel walls determines the knot size. The metastable knot size in weak confinement is larger than the one in bulk because the segments in the knot core experience less confinement free energy than the ones in the unknotted subchains. This result means the channel acts to push segments into the knot to reduce the total confinement free energy. On the other hand, the metastable knot size in strong confinement is smaller than the one in bulk because the segments in the knot core experience more confinement free energy. Here, the channel acts to expel segments from the core of the knot.

■ ASSOCIATED CONTENT

Supporting Information

The authors declare no competing financial interest. This material is available free of charge via the Internet at http://pubs.acs.org.

■ AUTHOR INFORMATION

Corresponding Author

*E-mail: pdoyle@mit.edu (P.S.D.).

Author Contributions

L.D. and C.B.R. contributed equally.

Notes

The authors declare no competing financial interest.

■ ACKNOWLEDGMENTS

This research was supported by the National Research Foundation Singapore through the Singapore MIT Alliance for Research and Technology's research program in BioSystems and Micromechanics, the National Science Foundation grant CBET-1335938. The authors thank the center for computational science and engineering in National University of Singapore for providing computational resources.

■ REFERENCES

(1) Tubiana, L.; Rosa, A.; Fragiacomo, F.; Micheletti, C. *Macromolecules* **2013**, *46*, 3669.
(2) Saitta, A. M.; Soper, P. D.; Wasserman, E.; Klein, M. L. *Nature* **1999**, *399*, 46−48.
(3) Farago, O.; Kantor, Y.; Kardar, M. *Europhys. Lett.* **2002**, *60*, 53.
(4) Kivotides, D.; Wilkin, S. L.; Theofanous, T. G. *Phys. Rev. E: Stat., Nonlinear, Soft Matter Phys.* **2009**, *80*, 041808.
(5) Renner, C. B.; Doyle, P. S. *Soft Matter* **2015**, *11*, 3105−3114.
(6) Taylor, W. R.; Lin, K. *Nature* **2003**, *421*, 25.
(7) Arsuaga, J.; Vazquez, M.; McGuirk, P.; Trigueros, S.; Sumners, D.; Roca, J. *Proc. Natl. Acad. Sci. U. S. A.* **2005**, *102*, 9165−9169.
(8) Ercolini, E.; Valle, F.; Adamcik, J.; Witz, G.; Metzler, R.; De Los Rios, P.; Roca, J.; Dietler, G. *Phys. Rev. Lett.* **2007**, *98*, 058102.
(9) Katritch, V.; Olson, W. K.; Vologodskii, A.; Dubochet, J.; Stasiak, A. *Phys. Rev. E* **2000**, *61*, 5545−5549.
(10) Mobius, W.; Frey, E.; Gerland, U. *Nano Lett.* **2008**, *8*, 4518−4522.
(11) Zheng, X.; Vologodskii, A. *Phys. Rev. E* **2010**, *81*, 041806.
(12) Grosberg, A. Y.; Rabin, Y. *Phys. Rev. Lett.* **2007**, *99*, 217801.
(13) Dai, L.; Renner, C. B.; Doyle, P. S. *Macromolecules* **2014**, *47*, 6135−6140.
(14) Dai, L.; Renner, C. B.; Doyle, P. S. *Phys. Rev. Lett.* **2015**, *114*, 037801.
(15) Mai, D. J.; Brockman, C.; Schroeder, C. M. *Soft Matter* **2012**, *8*, 10560−10572.
(16) Reisner, W.; Pedersen, J. N.; Austin, R. H. *Rep. Prog. Phys.* **2012**, *75*, 106601.
(17) Dai, L.; Van der Maarel, J. R. C.; Doyle, P. S. *Macromolecules* **2014**, *47*, 2445.
(18) Dai, L.; Jones, J. J.; van der Maarel, J. R. C.; Doyle, P. S. *Soft Matter* **2012**, *8*, 2972−2982.
(19) Dai, L.; Tree, D. R.; van der Maarel, J. R.; Dorfman, K. D.; Doyle, P. S. *Phys. Rev. Lett.* **2013**, *110*, 168105.
(20) Wang, Y.; Tree, D. R.; Dorfman, K. D. *Macromolecules* **2011**, *44*, 6594−6604.
(21) Cifra, P.; Benkova, Z.; Bleha, T. *Faraday Discuss.* **2008**, *139*, 377−392.
(22) Tang, J.; Levy, S. L.; Trahan, D. W.; Jones, J. J.; Craighead, H. G.; Doyle, P. S. *Macromolecules* **2010**, *43*, 7368−7377.
(23) Reisner, W.; Morton, K. J.; Riehn, R.; Wang, Y. M.; Yu, Z.; Rosen, M.; Sturm, J. C.; Chou, S. Y.; Frey, E.; Austin, R. H. *Phys. Rev. Lett.* **2005**, *94*, 196101.
(24) Balducci, A.; Mao, P.; Han, J.; Doyle, P. S. *Macromolecules* **2006**, *39*, 6273−6281.
(25) Tegenfeldt, J. O.; Prinz, C.; Cao, H.; Chou, S.; Reisner, W. W.; Riehn, R.; Wang, Y. M.; Cox, E. C.; Sturm, J. C.; Silberzan, P. *Proc. Natl. Acad. Sci. U. S. A.* **2004**, *101*, 10979−10983.
(26) Bonthuis, D. J.; Meyer, C.; Stein, D.; Dekker, C. *Phys. Rev. Lett.* **2008**, *101*, 108303.
(27) Gupta, D.; Sheats, J.; Muralidhar, A.; Miller, J. J.; Huang, D. E.; Mahshid, S.; Dorfman, K. D.; Reisner, W. *J. Chem. Phys.* **2014**, *140*, 214901.
(28) Dai, L.; van der Maarel, J. R. C.; Doyle, P. S. *ACS Macro Lett.* **2012**, *1*, 732−736.
(29) Micheletti, C.; Orlandini, E. *Macromolecules* **2012**, *45*, 2113−2121.
(30) Micheletti, C.; Orlandini, E. *Soft Matter* **2012**, *8*, 10959.
(31) Nakajima, C. H.; Sakaue, T. *Soft Matter* **2013**, *9*, 3140.
(32) Arai, Y.; Yasuda, R.; Akashi, K.-i.; Harada, Y.; Miyata, H.; Kinosita, K.; Itoh, H. *Nature* **1999**, *399*, 446−448.
(33) Bao, X. R.; Lee, H. J.; Quake, S. R. *Phys. Rev. Lett.* **2003**, *91*, 265506.
(34) Metzler, R.; Reisner, W.; Riehn, R.; Austin, R.; Tegenfeldt, J. O.; Sokolov, I. M. *Europhys. Lett.* **2006**, *76*, 696.
(35) Lam, E. T.; Hastie, A.; Lin, C.; Ehrlich, D.; Das, S. K.; Austin, M. D.; Deshpande, P.; Cao, H.; Nagarajan, N.; Xiao, M. *Nat. Biotechnol.* **2012**, *30*, 771−776.
(36) Levy, S. L.; Craighead, H. G. *Chem. Soc. Rev.* **2010**, *39*, 1133−1152.
(37) Persson, F.; Tegenfeldt, J. O. *Chem. Soc. Rev.* **2010**, *39*, 985−999.
(38) Reifenberger, J.; Dorfman, K.; Cao, H. *Bull. Am. Phys. Soc.* **2014**, in press.
(39) Jun, S.; Thirumalai, D.; Ha, B. Y. *Phys. Rev. Lett.* **2008**, *101*, 138101.
(40) Tubiana, L.; Orlandini, E.; Micheletti, C. *Prog. Theor. Phys. Suppl.* **2011**, *191*, 192.

DOI: 10.1021/acs.macromol.5b00280
Macromolecules 2015, 48, 2812−2818

(41) Frankkamenetskii, M. D.; Vologodskii, A. V. *Sov. Phys. Usp.* **1981**, *24*, 679−696.
(42) Marcone, B.; Orlandini, E.; Stella, A. L.; Zonta, F. *Phys. Rev. E* **2007**, *75*, 041105.

DOI: 10.1021/acs.macromol.5b00280
Macromolecules 2015, 48, 2812−2818